

## Step-Mountain Technique Applied to an Atmospheric C-Grid Model, or How to Improve Precipitation near Mountains

GARY L. RUSSELL

*NASA Goddard Institute for Space Studies, New York, New York*

(Manuscript received 10 October 2006, in final form 6 March 2007)

### ABSTRACT

Starting with Arakawa and Lamb's second-order C-grid scheme, this paper describes the modifications made to the dynamics to create a C-grid atmospheric model with a variable number of cells for each vertical column. Where mountains exist, grid cells are discarded at the bottom of the column so that the mass per square meter of retained cells is more nearly equal to that of horizontally adjacent cells. This leads to the following chain of causes and effects: decreased mass variations reduce the numerically induced alternating patterns in the horizontal velocity components, which reduce erroneous vertical mass fluxes, which reduce erroneous precipitation. In addition, horizontal flows above mountains are smoother, the Ferrel cell is stronger, and the polar cell is better organized. The C-grid performs geostrophic adjustment best among the gridpoint schemes, being the most sensitive to condensation-released heating perturbations. It also overreacts more egregiously to numerical errors, particularly with respect to the vertical mass flux, and consequently is often not used. Mesinger et al. applied the step-mountain (eta coordinate) technique to an E-grid scheme with excellent results. Its application to the C-grid reduces numerical errors in the vertical mass flux resulting in improvements in precipitation and other quantities.

### 1. Introduction

Improving precipitation in climate models requires a rather lengthy journey. In gridpoint schemes of general circulation models, prognostic scalar quantities such as mass, temperature, humidity, and tracers are defined in the same grid cells, referred to as the primary grid. Arakawa categorized rectangular gridpoint dynamical schemes depending on where the prognostic vector quantities, eastward and northward velocities, are located with respect to the primary grid. On the A-grid, velocity values are centered on the primary grid. Center-difference A-grid schemes are seldom used because derivatives needed on the primary grid must be calculated from opposite cells that are two cells apart. Without additional smoothing or filtering, a perturbation that develops in one cell is spread over a checkerboard pattern, which is unrealistic.

On the B-grid, velocity values are centered at the corners of the primary grid. In Arakawa's (1972)

scheme, mass fluxes for advection of scalar quantities are calculated by averaging the velocity component perpendicular to the flow. Derivatives for the pressure gradient force are calculated by scalar differences of adjacent primary cells and then are averaged perpendicular to the velocity component being accelerated. This averaging is less detrimental than the averaging parallel to the velocity component that occurs in A-grid center-difference schemes.

On the C-grid, eastward velocities are centered on the eastern and western edges of primary grid cells and northward velocities are centered on the northern and southern edges. In Arakawa and Lamb's (1977) scheme, there is no averaging of the velocity components for mass fluxes or for the pressure gradient force. Thus, "the simulation of geostrophic adjustment is best with Scheme C" (Arakawa and Lamb 1977, p. 190). Unlike the A-grid and B-grid, the two components of horizontal velocity are staggered in space (centered at different locations), and consequently the Coriolis and metric terms may be calculated with more averaging and less precision on the C-grid.

The arrangement of variables on the E-grid can be viewed as a B-grid rotated 45° or as two independent C-grids that are offset from each other by a half cell in

---

*Corresponding author address:* Gary L. Russell, NASA Goddard Institute for Space Studies, 2880 Broadway, New York, NY 10025.

E-mail: gary.l.russell@nasa.gov

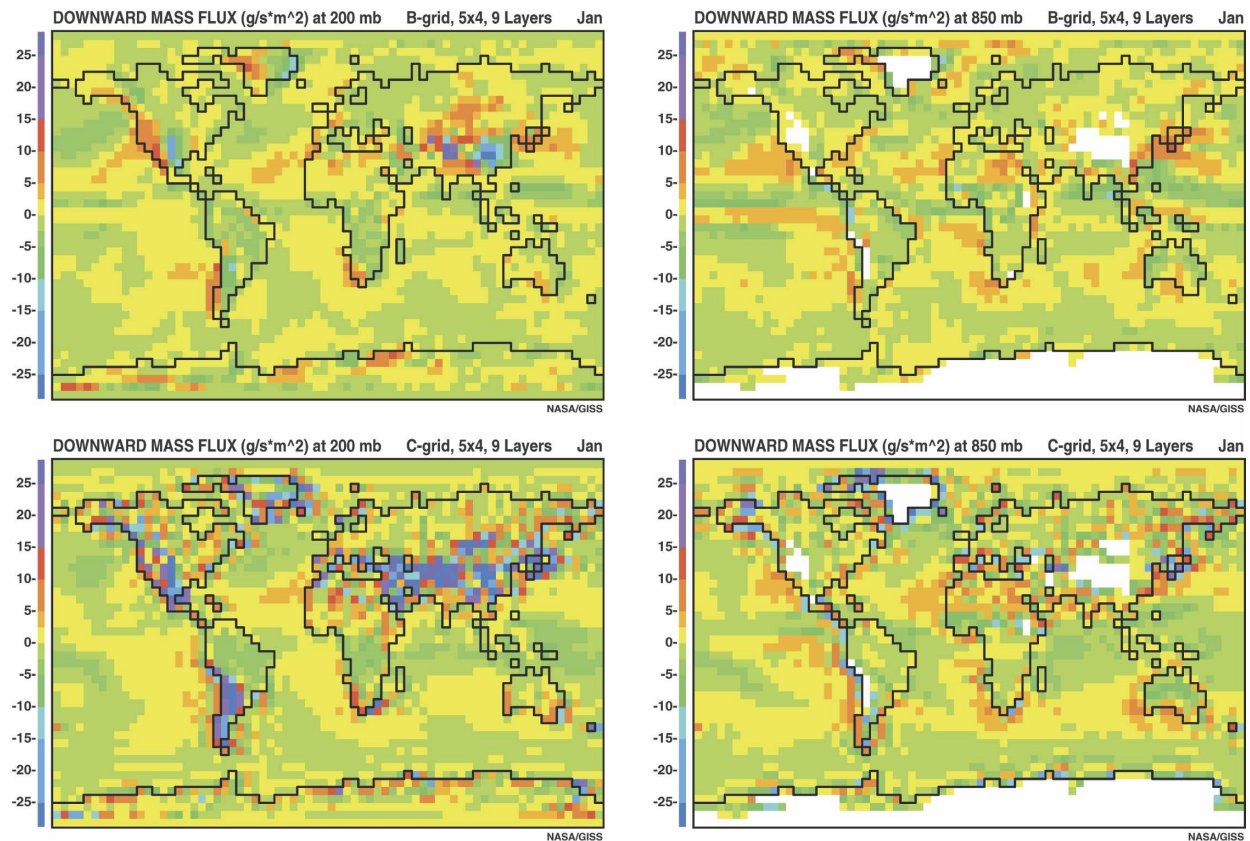


FIG. 1. Downward mass flux from earlier B-grid and C-grid models.

each horizontal direction. In Mesinger's (1981) scheme, eastward and northward velocity components reside at the same location, which is convenient for applying the Coriolis and metric terms. The pressure gradient force and the bulk of advection are applied to the separate C-grids, which can cause grid separation problems if not addressed. It is on the E-grid that Mesinger et al. (1988) first applied the step-mountain (eta coordinate) technique, discarding cells at the bottom of columns where mountains exist.

In years past, several different attempts were made at the Goddard Institute for Space Studies (GISS) to improve the flow near mountains (which is related to precipitation problems) without the step-mountain technique. None of them were successful. These included using Arakawa's (1966) fourth-order Jacobean in a C-grid general circulation model (Abramopoulos 1991) and using models that conserved potential enstrophy (Arakawa and Lamb 1981; Takano and Wurtele 1982; Abramopoulos 1988).

Mountains may generate erroneous vertical mass fluxes that result in erroneous precipitation. Figure 1 shows the vertical mass fluxes from B-grid and C-grid atmospheric general circulation models of the early

1990s vintage that used Arakawa's dynamical schemes. As a general rule of thumb, the B-grid scheme excites checkerboard patterns in the mass field whereas the C-grid scheme excites checkerboard patterns in the velocity components. The vertical mass flux is derived from the convergence of the horizontal velocities and is consequently sensitive to the velocity's alternating patterns. Thus, one would expect that checkerboarding in the vertical mass flux would be more extreme in the C-grid than in the B-grid, and this is confirmed by the figure. Because this checkerboarding is so much more extreme in the C-grid, one might expect that the B-grid should be a better model. In fact the two models are comparable in abilities, but if the erroneous vertical mass fluxes in the C-grid could be corrected, it should become the superior model.

This paper describes the changes and improvements made from Arakawa and Lamb's (1977) C-grid algorithms culminating in the step-mountain implementation. The modifications were that the second-order differencing scheme for the linear advection of tracer quantities, which was numerically inaccurate, was replaced by the linear upstream scheme; both potential enthalpy and specific humidity now require three direc-

tional gradients as well as mean values inside each cell (section 2). Half of the corner fluxes in the advection of momentum were eliminated; this allowed the mass stencil, the combination of mass cells that converts a velocity value to momentum, to be reduced from six mass cells to two (section 3). The Coriolis and metric terms for the eastward component of velocity now conserve angular momentum by advection; the Coriolis and metric terms for the northward component conserve kinetic energy in concert with the eastward component (section 4). For the pressure gradient force, geopotential height and enthalpy are mass weighted within each layer using the prognostic vertical gradient of heat, and cell distances are defined specifically for this term (section 5). At each pole, a single horizontal velocity vector was defined that rotationally sends and receives advective fluxes and is accelerated by the pressure gradient forces around the pole (section 6). A hybrid vertical coordinate is defined in which each layer has a fixed amount of mass plus a fixed fraction of a variable column mass (section 7). The step-mountain technique is implemented; cells are discarded at the bottom of a column so that the mass per unit area of cells above the mountain is more nearly equal to horizontally adjacent cells of the same layer (section 8). Continental topography is adjusted as a further refinement in forcing the mass per unit area of adjacent cells to be more nearly equal (section 9). Results, the improvement in precipitation (section 10), and a discussion (section 11) follow.

## 2. Linear upstream scheme replaces second-order differencing for linear advection

Atmospheric advection is the transport of a quantity through the air via the winds. Linear advection is the transport of a quantity other than the winds; nonlinear advection is the transport of momentum or the winds themselves. Center-difference schemes for linear advection are not as good as intelligent upstream schemes (described later) when the mass of each grid cell is constant. When mass variations increase (because of mountains), an advected structure degrades more rapidly in a center-difference scheme than in an intelligent upstream scheme (Russell and Lerner 1981). Spectral advection schemes suffer the same fate as do center-difference schemes.

To understand why the above degradation occurs requires understanding what is the natural coordinate system of a tracer quantity. Tracer concentration is defined as tracer mass in a parcel divided by air mass in the parcel. Integrated air mass, in each of the three directions, is the natural coordinate system because dif-

ferences in the airmass coordinates determine the denominator when tracer concentration is measured. In the vertical direction, integrated air mass is proportional to pressure (assuming constant gravity). If a sine wave was sampled at irregular points and then a center-difference or spectral advection operator was applied, the result would not be very smooth. This problem develops when a tracer field is sampled at even intervals in space but in irregular intervals in the natural airmass coordinate; the advection operator erroneously assumed that the tracer values were evenly distributed. The magnitude of the errors depends on how large the variation is between the spatial coordinate used and a natural airmass coordinate. Mountain-induced airmass variations exist indefinitely in time and cause persistent systematic degradation of advected fields.

Upstream advection schemes do not require that a tracer field be equally distributed in its coordinate system and are relatively immune to mass variations. The standard scalar upstream scheme is known to be highly diffusive, but intelligent upstream schemes for linear advection do exist (Van Leer 1977), and among them are the linear upstream scheme (Russell and Lerner 1981) and the quadratic upstream scheme (Prather 1986). Before upstream schemes were implemented at GISS, persistent “zeroes” occurred in the humidity field at a few locations, which was not conducive to good precipitation.

The linear upstream scheme is used for linear advection in the resultant model here, being a compromise between little diffusion and reduction in complexity, disk space, and computing time. Each scalar quantity (heat, humidity, and other tracers) on a primary grid cell contains three directional gradients and a mean value, all of which are prognostic variables with time derivatives. The gradients participate in and are updated by the advection scheme. In addition, primary grid cells are subdivided into  $\frac{1}{4}$  or  $\frac{1}{8}$  grid cells upon which condensation subroutines are applied.

The resultant dynamical model of this paper still uses a second-order center-differencing scheme for nonlinear advection that suffers the same deficiencies as mentioned above for linear advection. Lin and Rood (1997) have developed a semi-Lagrangian (upstream) scheme for nonlinear advection that has been tested at different modeling centers. It could conceivably make an improvement in the resultant model here. The errors generated by the center-difference momentum advection scheme are reduced compared to prior versions because the present resultant model discards mountainous cells at the bottom of a column and the continental topography may be adjusted so that the airmass variations are minimized. In C-grid schemes at GISS, alter-

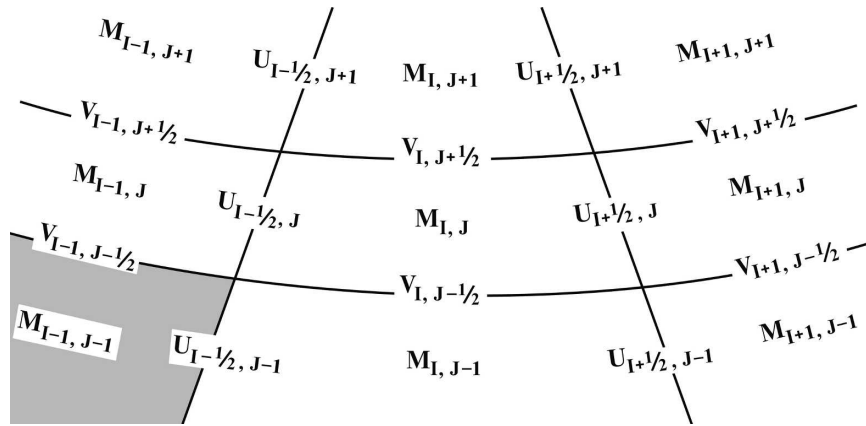


FIG. 2. Arrangement of variables for the C-grid: mass  $M$  ( $\text{kg m}^{-2}$ ) along with other scalar quantities is defined on primary grid cells; eastward velocity  $U$  ( $\text{m s}^{-1}$ ) and northward velocity  $V$  ( $\text{m s}^{-1}$ ) are centered at the edges of primary grid cells. The eastward mass flux is centered where  $U$  is, and the northward mass flux is centered where  $V$  is. If the primary cell  $(I - 1, J - 1)$  is a discarded mountainous cell, then  $U_{I-1/2, J-1}$  and  $V_{I-1, J-1/2}$  would be set to zero in the present resultant model. With Arakawa and Lamb's (1977) six-cell mass stencil, both  $U_{I-1/2, J}$  and  $V_{I, J-1/2}$ , when converting to momentum, would attempt to use  $M_{I-1, J-1}$ , which is not defined.

nating patterns of the velocity components are filtered in the zonal direction while conserving angular momentum.

### 3. Half of the corner fluxes in momentum advection are eliminated

Most three-dimensional gridpoint schemes on the sphere solve the primitive equations, which are given in flux form and discretized in the vertical in appendix A. The arrangement of the variables, the order of the scheme, and other factors cause wide variations in a scheme's algorithmic solution and behavior. The finite-difference algorithms for mass and momentum for this paper's resultant model are given in appendix B. It is desirable that properties including mass and energy are conserved by various processes. In Arakawa and Lamb's (1977, p. 204) second-order C-grid discretization of the primitive equations, corner fluxes of momentum are needed in order to conserve enstrophy under nondivergent flow. Atmospheric flow, however, is divergent, so enstrophy is not conserved exactly, but this nondivergent property in Arakawa's differencing schemes has other benefits, namely to control the cascade of kinetic energy to smaller scales.

Arrangement of variables for the C-grid is described in Fig. 2. Using  $U$  for the eastward velocity and  $V$  for the northward velocity, the corner flux of eastward momentum needed for enstrophy conservation has two mass flux components that multiply the average of  $U_{I-1/2, J}$  and  $U_{I+1/2, J+1}$  in Arakawa and Lamb. The first

component is a four-point average of eastward mass fluxes and the second component is a single northward mass flux. The modification made here is to eliminate the first component. Similarly, when the corner flux of northward momentum from  $V_{I, J-1/2}$  to  $V_{I+1, J+1/2}$  is calculated, the four-point average of northward mass fluxes is eliminated. There are two reasons for this simplification: the mass stencil that multiplies velocity to obtain momentum can be reduced from six mass cells to two, and angular momentum can be conserved while maintaining the conservation of kinetic energy by the Coriolis and metric terms.

If the full momentum corner fluxes are used as in Arakawa and Lamb, then in order to maintain uniform flow over a large domain, the mass stencil of  $U_{I+1/2, J}$  would require these six mass cells:  $M_{I, J-1}$ ,  $M_{I+1, J-1}$ ,  $M_{I, J}$ ,  $M_{I+1, J}$ ,  $M_{I, J+1}$ , and  $M_{I+1, J+1}$ . (Here  $M$  is the mass of a primary grid cell.) If the reduced momentum corner fluxes are used, then the mass stencil of  $U_{I+1/2, J}$  can be reduced to cells  $M_{I, J}$  and  $M_{I+1, J}$  and that of  $V_{I, J+1/2}$  to  $M_{I, J}$  and  $M_{I, J+1}$ . In general, it is preferable to localize the interaction among variables so that a variable affects other variables only in its immediate vicinity and not variables that are farther away.

The resultant scheme with reduced corner fluxes and the two-cell mass stencil is called the simplified advection scheme. It was tested with the improved Coriolis and metric terms (section 4) in a  $4^\circ \times 3^\circ$ , 12-layer model. Based on 10-yr simulations and comparisons with 50 observational fields, the results were just as good as using the Arakawa and Lamb scheme. Never-

theless, enstrophy is conserved less accurately during nondivergent flow. Integrating the simplified advection scheme with improved Coriolis and metric terms at  $4^\circ \times 3^\circ$  in a 1-layer shallow water equation model with Rossby–Haurwitz wave-4 initial conditions, the simulation diverges after 75 days. The Arakawa and Lamb scheme does not diverge. In a climate model, source terms and a filter on the velocity components (that were not used for the shallow water equations) will overwhelm the slow loss of enstrophy conservation.

When step-mountain mass cells are discarded in the resultant C-grid scheme, a velocity component is only nonzero if both of its mass cells contain air. If one of the two mass cells is discarded, then the velocity component is perpendicular to the face of a mountain, and it is set to zero. If the six-cell mass stencil were in use, one or more of the mass cells may have been discarded although the velocity component may want to be nonzero (Fig. 2). The mass stencil for B-grid and E-grid schemes use four mass cells. If one of the four has been discarded, then the velocity point is at the corner of a mountain and various inelegant decisions need to be made: should both velocity components be set to zero or should the mass weighting be altered? A similar problem arises when two of the four mass cells have been discarded.

#### 4. Angular momentum is conserved by advection and the Coriolis and metric terms

To conserve the axis component of angular momentum by advection and the Coriolis and metric terms, a definition of angular momentum is needed for the C-grid:

$$A_{I+1/2,J} = \Omega R^2 \text{COSQ}_J^2 + R \text{COSM}_J U_{I+1/2,J}, \quad (4.1)$$

where  $A$  ( $\text{m}^2 \text{s}^{-1}$ ) is the axis component of angular momentum per unit mass,  $\Omega$  ( $\text{s}^{-1}$ ) is the angular rotation rate of the earth,  $R$  (m) is the radius of the earth,  $\text{COSQ}$  and  $\text{COSM}$  are two specific definitions of cosine of latitude, and  $J$  is the gridcell index of latitude. The advection algorithm of section 3 (ignoring the Coriolis and metric terms) conserves linear eastward momentum. This algorithm is applied to  $A$ , which, consequently, is conserved. When  $A$  is replaced by the right-hand side of (4.1), the terms of the algorithm's application break into the advection algorithm applied to  $U$ , the Coriolis term, and the metric term, all multiplied by  $R \text{COSM}_J$ . This process could have been accomplished with the full corner fluxes and the six-cell mass stencil, but it is complicated and was never programmed. This technique was only implemented for the simplified advection scheme. The solution is given in appendix B and

the derivation is available online (see <http://aom.giss.nasa.gov/doc4x3.html>).

There is some freedom in choosing the cosines,  $\text{COSQ}$  and  $\text{COSM}$ , but some choices are superior to others. The choices selected for the resultant model are simple and were found to be as good as or better than other possibilities that were considered. Another wrinkle that is divulged in the derivation is that when angular momentum is advected northward from one primary latitude row to another, the exact cosine of latitude of the cell edges is used. Again, other choices are possible, but this is what was selected. This wrinkle violates exact conservation, but the global change of angular momentum due to advection (including the Coriolis and metric terms) is four orders of magnitude smaller than that due to either the pressure gradient force or due to surface friction.

With the reduced corner fluxes, each term of the Coriolis and metric terms that affects eastward momentum (UM) in Eq. (A2) contains a linear factor of  $V$ . (With Arakawa and Lamb's full corner fluxes, this is not the case, and it is the reason that they do not attempt to conserve angular momentum.) Each term of the Coriolis and metric terms that affects northward momentum (VM) in Eq. (A.3) is designed to contain a linear factor of  $U$ , and when the Coriolis and metric terms of UM are multiplied by  $U$  they cancel a term in the designed VM equation multiplied by  $V$ . Summing all changes to  $\text{UM} \times U + \text{VM} \times V$  over the globe, the Coriolis and metric terms all cancel exactly. Except for variations in mass, the Coriolis and metric terms therefore conserve kinetic energy.

#### 5. Changes made to the pressure gradient force

With only mean potential temperature defined over a layer, there are different choices that can be made in calculating the geopotential height; should potential temperature be constant throughout the layer, should temperature be constant throughout the layer, or should some other choice be made? This is the debate that occurred in Arakawa and Lamb (1977, p. 234), and their answer is not completely satisfactory. In GISS models and the present resultant model, both the mean and the vertical gradient of potential enthalpy (potential temperature  $\times$  mass  $\times$  constant specific heat capacity) are prognostic variables, and assuming these two values to be exact, temperature is known at every depth of a layer. Both the geopotential thickness and the mass-weighted height of a layer are calculated by integration from the well-defined (but not continuous) temperature function. The finite-difference algorithm is given in appendix C.

On a rectangular flat domain, the distances used in the denominator of the pressure gradient force are straightforward, but on a longitude–latitude spherical domain they are not obvious. For the resultant model, the east–west distance (m), which is used in the denominator when accelerating the eastward velocity [Eq. (C.2)], is

$$\Delta XPGF_J = R\Delta\lambda \int \cos^2(\varphi) d\varphi / \int \cos(\varphi) d\varphi, \quad (5.1)$$

where  $\Delta\lambda$  is the east–west angular distance of a grid cell in radians and the integrals are performed with respect to latitude from the southern edge to the northern edge of a primary grid row  $J$  (cells at same latitude). The interpretation of Eq. (5.1) is that the ratio of the integrals is the area-weighted cosine of latitude and  $\Delta XPGF$  is the area-weighted east–west distance. The north–south distance (m), which is used in the denominator when accelerating the northward velocity [Eq. (C.3)], is

$$\Delta YPGF_{J+1/2} = R(\Phi_{J+1} - \Phi_J), \quad (5.2)$$

where  $\Phi_J$  is the area-weighted latitude in radians of a primary grid cell.

These formulas were determined by trial and error by the following test. A one-layer shallow water equations model on a sphere without topography or rotation ( $\Omega = 0$ ) was initialized by a height field that was a linear function of the distance along the sphere from a point on the equator. The initial acceleration from this height field was calculated in closed form, and then was area averaged over the C-grid velocity cells. This closed form acceleration was compared with that generated by the shallow water model with different formulas for  $\Delta XPGF$  and  $\Delta YPGF$ . The Eqs. (5.1) and (5.2) were deemed satisfactory; the distances of Arakawa and Lamb were worse.

## 6. A single horizontal velocity vector is defined at each pole

In Arakawa and Lamb (1977), polar caps for the North and South Poles were defined so that all scalar quantities defined on triangular grid cells touching the same pole would have the same value. This procedure is continued still. What is new is how velocities are defined at the poles. Arakawa and Lamb did not define a separate eastward velocity at the primary grid row touching a pole, but the mass of the polar cap was given full weight when converting  $U$  velocity to  $U$  momentum at the grid row adjacent to a pole as though that same

velocity were defined over both grid rows. Similarly, the northward velocity edging a polar grid cell receives the full weight of the polar cap whereas at other latitudes it would receive only half the weight of the grid rows it edges. This method was unsatisfactory because the flow around and across a pole was not very smooth and the model would diverge about every 20 yr of integration with the time step used ( $2 \times 5$  min for the leapfrog time scheme of the  $4^\circ \times 3^\circ$  model).

This method is replaced by defining a single two-component horizontal velocity vector for each polar cap. Eastward velocity of the polar grid row has a sine wave appearance in longitude when interacting with grid cells adjacent to the pole. Northward velocity touching the pole also has a sine wave appearance that is  $90^\circ$  out of phase with the eastward component. Each momentum component sends and receives advective fluxes and participates in Coriolis and metric term calculations. After the advection step, the eastward momentum cells in each polar grid row are spectrally analyzed and the sine and cosine coefficients of wavenumber-1 are used to determine the next velocity vector at the pole. The northward momentum cells at a pole have half as much mass as do the eastward momentum cells at the pole and are discarded.

In the C-grid, northward velocity cells are centered between two primary grid rows. The pressure gradient force that acts on northward velocity cells edging a pole are based on values of mass and potential enthalpy of the polar cap minus that of primary grid cells adjacent to the pole. These gradients are spectrally analyzed using all longitudes, and the sine and cosine coefficients of wavenumber 1 are retrieved and are applied as the pressure gradient force acting on the polar vector velocity with the appropriate distance factor.

Since implementing this modification to the poles, simulations no longer diverge, and flow around and across the poles is much smoother. This improvement was confirmed in tests made with the one-layer shallow water equations model; it eliminated alternating patterns that develop at the poles.

## 7. Vertical layering is a combination of constant mass and a sigma coordinate

The vertical coordinate at any level of the resultant model is neither sigma nor eta but the mass per unit area above the level. If gravity is constant, this coordinate is proportional to pressure. The vertical layering is maintained by the vertical mass fluxes that are forced by the horizontal mass fluxes.

Arakawa and Lamb (1977) used fixed pressure layers between the model top and a fixed intermediate pres-

sure level  $P_I$  (approximately the tropopause) and a pure sigma coordinate system between  $P_I$  and the surface. Because water vapor mass was ignored in the atmosphere and the sigma coordinates were fixed, the vertical layering was determined by a two-dimensional horizontal pressure array. At GISS, mass per unit area (which includes water vapor) is a three-dimensional prognostic variable given by (A.1), and the vertical layering is more general: each layer has a fixed amount of mass [MFIX ( $\text{kg m}^{-2}$ )], plus a fixed fraction (MFRAC) of a column variable amount. The columns headed by MFIX and MFRAC in Table 1 are constant global numbers for a model simulation. For each grid column, the column variable amount ( $\text{kg m}^{-2}$ ) is

$$\text{MVAR} = \text{MSURF} - \text{MTOP} - \sum \text{MFX}_K, \quad (7.1)$$

where MSURF is the total mass per unit area of the column, MTOP is the fixed mass above the dynamical top, and the summation of  $K$  is taken over nondiscarded layers in the column. The prognostic mass per unit area of a layer  $L$  is

$$M_L \equiv \text{MFX}_L + \text{MFRAC}_L \text{MVAR} / \sum \text{MFRAC}_K, \quad (7.2)$$

where again the summation of  $K$  is taken over nondiscarded layers in the column.

Precipitation and evaporation remove or add mass to individual layers so that after the source terms, the variable mass of each layer,  $M_L - \text{MFX}_L$ , in a column may no longer be proportional to the MFRACs. The subroutine that calculates vertical mass fluxes, however, smoothly adjusts the mass of grid cells in each column during the dynamics so that at the end of the dynamics, the variable mass of individual layers are exactly proportional to the MFRACs. The sum of the MFRACs need not equal 1; it is the relative ratios that are important.

The vertical resolution displayed in Table 1 is not appropriate for a model with a fixed number of layers everywhere. Over the Himalayas in such a model, MSURF may be as low as  $5300 \text{ kg m}^{-2}$ , which means MVAR would be  $-2500 (=5300 - 100 - 7700)$  and the mass in layers 7 through 11 would be  $87.5 (=400 - 2500 \times 4/32)$ . Such thin layers could cause numerical problems.

MFIX and MFRAC of Table 1 are used for the 20-layer resultant model developed here. With a variable number, LM, of layers in a column, only the first LM values of MFIX and MFRAC are used, but for every grid column the mass of a layer is quite close to that entered under column  $M$ . Another consideration was to

TABLE 1. Vertical resolution for a 20-layer atmosphere. Layers are counted from the top downward. MFIX ( $\text{kg m}^{-2}$ ) is the fixed amount of mass in each layer. MFRAC is the fraction of the column's variable mass (that may be negative) that is added to each layer. MTOP =  $100 \text{ kg m}^{-2}$ , the fixed amount of mass above the dynamical model top. The contents of columns headed by MVAR (variable mass of individual layers),  $M$  (total mass of layers), and VSUM (vertically integrated  $M$ ) are for a sample grid column with 20 layers whose total column mass is  $10\,360 \text{ kg m}^{-2}$ , about 1016 mb.

Layer	MFIX	MFRAC	MVAR	$M$	VSUM
					100
1	200	0	0	200	300
2	300	0	0	300	600
3	400	0	0	400	1000
4	400	1/32	80	480	1480
5	400	2/32	160	560	2040
6	400	3/32	240	640	2680
7	400	4/32	320	720	3400
8	400	4/32	320	720	4120
9	400	4/32	320	720	4840
10	400	4/32	320	720	5560
11	400	4/32	320	720	6280
12	400	3/32	240	640	6920
13	400	2/32	160	560	7480
14	400	1/32	80	480	7960
15	400	0	0	400	8360
16	400	0	0	400	8760
17	400	0	0	400	9160
18	400	0	0	400	9560
19	400	0	0	400	9960
20	400	0	0	400	10360
	7700	32/32	2560	10260	

have the lowest layer, where surface interaction occurs, nearly the same for all grid columns. Less than 5% of the area of the earth has mountains that would occupy layer 14.

## 8. Allow a variable number of layers, implement a step-mountain technique

The model with a variable number of layers requires two new input files. The LM file fixes the number of layers for each horizontal grid column, and a second file contains offline calculations used by the model's polar filter. The atmospheric initial conditions input file is recreated by a modified offline program that reads the LM file. This program and the model itself were tested first with an LM file that had the same fixed number of layers everywhere.

The LM file must be created first. Each primary grid column lies above a surface cell that is either all ocean or all continent. In the atmosphere above an ocean cell, the number of layers is always the fixed maximal number. The principle to be followed over continental columns is to choose the number of layers so that the mass per unit area of a cell is as close as possible to the

average mass of its eight horizontally surrounding cells of the same layer. If the number of layers of a column obeys this principle for a particular layer, then the principle is obeyed for other layers of the column. The principle is implemented by changing the number of layers iteratively; the column that is most out of line with its neighbors is corrected first. Columns may be corrected more than once during the process. The advantage of using the above principle, as opposed to choosing the number of layers independent of neighboring columns, is that it minimizes the discrepancy in mass with horizontally adjacent cells.

Unfortunately, the above principle is insufficient to uniquely determine the number of layers over the continents; the solution depends upon the initial guess. Starting with the ocean maximal number of layers everywhere (method 1) produces a solution with the fewest number of discarded cells that are consistent with the principle. Another starting method is to spread the mass of each layer from the oceans smoothly over the continents, defining an ideal mass (the average mass of its horizontal neighbors) for each continental cell with the full maximal number of layers everywhere and temporarily ignoring the mountains. Then, for each continental column, choose  $N$  (which will become the first guess for the number of layers) so that the sum of the first  $N$  ideal masses is closest to the column's actual column mass (method 3). Intermediate starting values are also possible (method 2). Note that the column mass comes from a prior simulation, and over the ocean it may vary within  $250 \text{ kg m}^{-2}$ . From the ocean masses of a layer, ideal continental masses are generated by a smooth unique convergent solution.

The polar filter is used to allow a longer dynamical time step than would otherwise be needed. The eastward mass flux and the east–west pressure gradient force are Fourier analyzed in longitude, and spectral coefficients of each field are multiplied by the factor SMOOTH [Arakawa and Lamb 1977, p. 250, their Eq. (325)], which is a function of wavenumber and latitude and is limited to 1:

$$\text{SMOOTH} = \Delta X / [\Delta Y \sin(\pi N / \text{IM})], \quad (8.1)$$

where  $\Delta X$  is the east–west gridcell distance (a function of latitude),  $\Delta Y$  is the north–south gridcell distance, IM is the number of east–west grid cells around the globe, and  $N$  is the wavenumber (which is limited to  $\text{IM}/2$ ). In the present resultant model, the same two fields are filtered with the same strength when a primary grid row of a given layer is above the mountains, but when a primary grid row intersects a mountain, the row is broken into one or more basins. A basin that is  $\text{KM}$  pri-

mary grid cells wide will have edges for  $\text{KM} - 1$  field values to be filtered. The field is Fourier analyzed on  $2 \times \text{KM}$  periodic values, which include zeroes on each coast and  $\text{KM} - 1$  reflected values of opposite sign. The cosine coefficients are all zero, but the sine coefficients are multiplied by the same SMOOTHing factor as in (8.1) except that IM is replaced by  $2 \times \text{KM}$  and the largest wavenumber is  $\text{KM} - 1$ . Because filtered field values are fixed linear combinations of the  $\text{KM} - 1$  unfiltered values, the matrix coefficients of linear combinations are calculated once in an offline program but are used repetitively in the atmospheric polar filter subroutine. The matrix coefficients depend upon  $\text{KM}$  and latitude ( $\Delta X$  and  $\Delta Y$ ).

## 9. Adjust continental topography after LM file has been determined

The object of using a variable number of layers is to cause the mass per unit area of any cell to be more nearly equal to its horizontally adjacent cells. A further refinement in achieving this goal is to adjust the continental topography of a simulation. The mass per unit area of each cell over the oceans is derived from a multiyear annual mass distribution from a prior simulation. These ocean masses are spread smoothly over the continents (as was done in method 3 of section 8), producing an ideal mass for every cell on land, discarded or not. The ideal column mass over the continents is the summation of the ideal masses over the nondiscarded layers as specified by the LM file. The ideal and the model's present column masses from the prior simulation are to be matched by adjusting the continental topography.

The multiyear simulation's column mass (MSURF) is subtracted from the ideal column mass to produce a discrepancy,  $\Delta M$  ( $\text{kg m}^{-2}$ ). Adjusting the continental topography by  $\Delta Z$  (m) in future simulations would cause their column mass to approach the ideal column mass:

$$\Delta Z = [1 - (1 + \Delta M / \text{MSURF})^{\gamma/\beta/G}] T / \beta, \quad (9.1)$$

where  $\gamma$  ( $\text{J kg}^{-1} \text{K}^{-1}$ ) is the gas constant for dry air,  $\beta$  ( $\text{K m}^{-1}$ ) is the moist-adiabatic lapse rate,  $G$  ( $\text{m s}^{-2}$ ) is the earth's gravitational acceleration, and  $T$  is the surface temperature (K) from the same prior simulation.

If the LM file from method 1 (least discarded cells) is chosen, then the area-weighted  $\Delta Z$  over the continents is  $-338$  m. Method 3 yields a continental  $\Delta Z$  of  $-17$  m. From the LM file of method 3, method 4 creates a new LM file in which more cells over the continents are discarded until the global mean mass of a layer matches

TABLE 2. Root-mean-square error of precipitation ( $\text{mm day}^{-1}$ ) over Northern Hemisphere ground for January and July. Five climatological observation files [Legates and Willmott (1990), years 1920–80; Shea (1986), years 1950–79; German Climate Research Programme (2005; DEKLIM), years 1951–2000; New et al. [1999; Climate Research Unit (CRU)], years 1961–90; Adler et al. [2003; Global Precipitation Climatology Project (GPCP)], years 1979–99] are compared among themselves and against 3 model simulations: (i) 20 layers everywhere; (ii) 20 layers maximum, method 1 of section 8 is used to determine the LM file; and (iii) 20 layers maximum, method 4 of section 9 is used to determine the LM file, and continental topography is adjusted.

	January					July				
	Legates	Shea	DEKLIM	CRU	GPCP	Legates	Shea	DEKLIM	CRU	GPCP
Legates	0	0.58	0.59	0.55	0.64	0	1.33	1.31	1.01	1.35
Shea	0.58	0	0.37	0.45	0.59	1.33	0	1.09	1.18	.96
DEKLIM	0.59	0.37	0	0.38	0.53	1.31	1.09	0	1.23	1.42
CRU	0.55	0.45	0.38	0	0.59	1.01	1.18	1.23	0	.98
GPCP	0.64	0.59	0.53	0.59	0	1.35	.96	1.42	.98	0
(i)	1.57	1.62	1.63	1.64	1.64	2.85	2.57	2.78	2.63	2.52
(ii)	1.02	0.94	0.94	0.97	0.89	2.32	1.98	2.23	2.03	1.80
(iii)	1.13	0.99	1.01	1.05	0.91	2.65	2.25	2.56	2.30	1.98

the global mean ideal mass. Method 4 yields a continental  $\Delta Z$  of a little more than +1 m.

## 10. Results

The results of this section relate to three 12-yr simulations of recent  $4^\circ \times 3^\circ$  atmospheric models: (i) 20 layers everywhere; (ii) 20 layers maximum, method 1 of section 8 is used to determine the LM file; and (iii) 20 layers maximum, method 4 of section 9 is used to determine the LM file, and continental topography is adjusted. Comparisons are made using the last 10 yr. Simulation (i) has different values for MFIX and MFRAC; MFIX is less than those given by Table 1. The relationship between cloud optical depths and mass of condensate were tuned for each simulation in order to optimize the comparisons with observations. Other minor parameters were also tuned. Actually, each model was simulated 8 times with slightly varying initial temperatures, and the best simulation was chosen for the subsequent results. Each group of eight simulations is quite similar; the root-mean-square error in precipitation in Table 2 (discussed later) between the best and worst simulations is about  $0.08 \text{ mm day}^{-1}$ .

Other than the vertical layering and tuning, the three simulations use identical coding. Each tries to reproduce the climatology of the second half of the twentieth century using climatologically observed ocean surface temperatures and sea ice distributions. A common feature is a filter that conserves momentum and is applied in the east–west direction to the horizontal velocity components. It is mentioned because it affects the dynamics—the topic of this paper. The strength of this filter can be weakened in simulations (ii) and (iii), but this was not done.

Numerically induced noise is present in the monthly

northward velocity of simulation (i) at all layers around mountains, but is nearly missing in (ii) and is absent in (iii) except possibly in the Himalayas. An alternating pattern in latitude develops at the surface above the ocean near Antarctica in simulations (ii) and (iii) that was not significant in (i). This is the only quantity and region that degrades; overall, northward velocity (which is not displayed) is smoother in simulations (ii) and (iii) than it is in (i).

Vertical mass fluxes in general are more sensitive than are horizontal velocities, and they are shown in Fig. 3 for January for 200- and 850-mb pressure levels. The numerical noise at 200 mb that is present in simulation (i) is reduced in (ii) and is nearly eliminated in (iii). In particular, the alternating pattern in South America, which is present in simulation (i) at 200 mb and also in the earlier B-grid and C-grid simulations of Fig. 1, is eliminated in (ii) and (iii). At 850 mb, rising air on the western side of the Rocky Mountains and sinking air on the eastern side are clearly indicated in (ii) and (iii), but not so in (i) nor in Fig. 1. Although the magnitudes of the vertical mass fluxes are reduced from (i), simulation (ii) is still more spotted than the B-grid of Fig. 1. Improvements in the vertical mass flux will pay big dividends in the precipitation field.

The maximum value of the January Northern Hemisphere Hadley cell is nearly identical in all three simulations: 194 in (i), 194 in (ii), and  $193 \times 10^9 \text{ kg s}^{-1}$  in (iii). The maximum value of the Ferrel cell is  $-30$  in (i),  $-40$  in (ii), and  $-49$  in (iii), and the cell is about  $3^\circ$  narrower in latitude in simulation (i). The polar cell is very disorganized in (i) and eventually a cell with the same sign as the Ferrel cell develops between  $68^\circ$  and  $85^\circ\text{N}$ . In the other simulations, the polar cell is well developed with a maximum value of 12 in (ii) and 9 in (iii) and which extends from about  $61^\circ$  to  $77^\circ\text{N}$ .

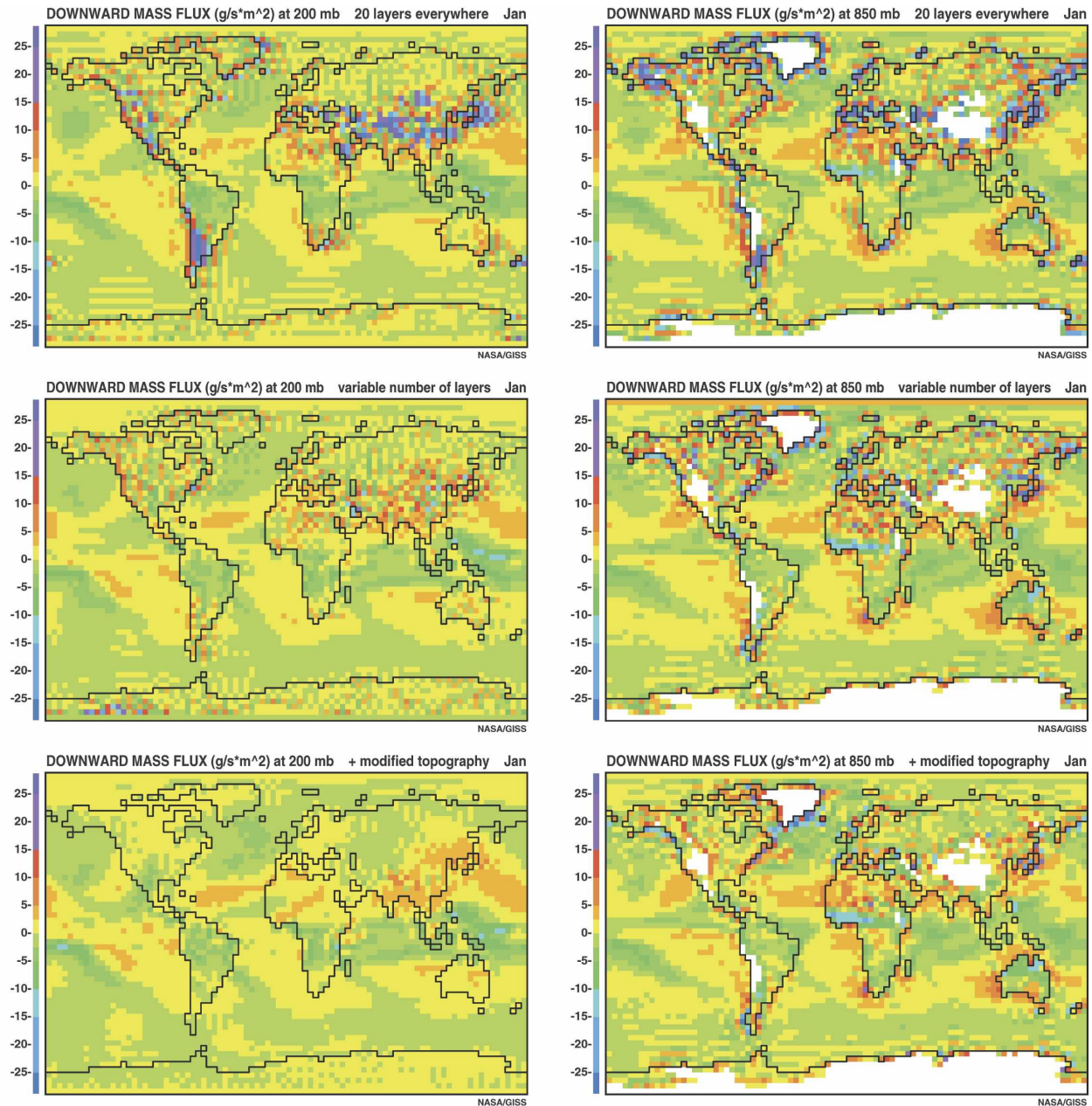


FIG. 3. Downward mass flux from simulations (i), (ii), and (iii).

Among quantities with adequate observations, precipitation shows the greatest improvement when step-mountain is used. Figure 4 shows the January and July precipitation for simulations (i) and (ii) and the observations of Shea (1986). Simulation (iii) is quite similar to (ii) and is not displayed. Precipitation peaks on Greenland, Iceland, and Norway of simulation (i) are reduced in (ii) and are then more similar to Shea. The largest improvement is in South America. The precipitation peaks in the northern Andes are eliminated in

(ii), and in the south, the precipitation that fell on the continent in (i) is moved to the Pacific Ocean in (ii) where it coincides with Shea.

Table 2 shows the root-mean-square error comparisons of model results versus five observational precipitation files over Northern Hemisphere ground; thus, much of South America is excluded from this comparison. The observational files were interpolated (conserving means) to the model's  $4^\circ \times 3^\circ$  resolution before comparing. Simulation (ii) is the most accurate. Note

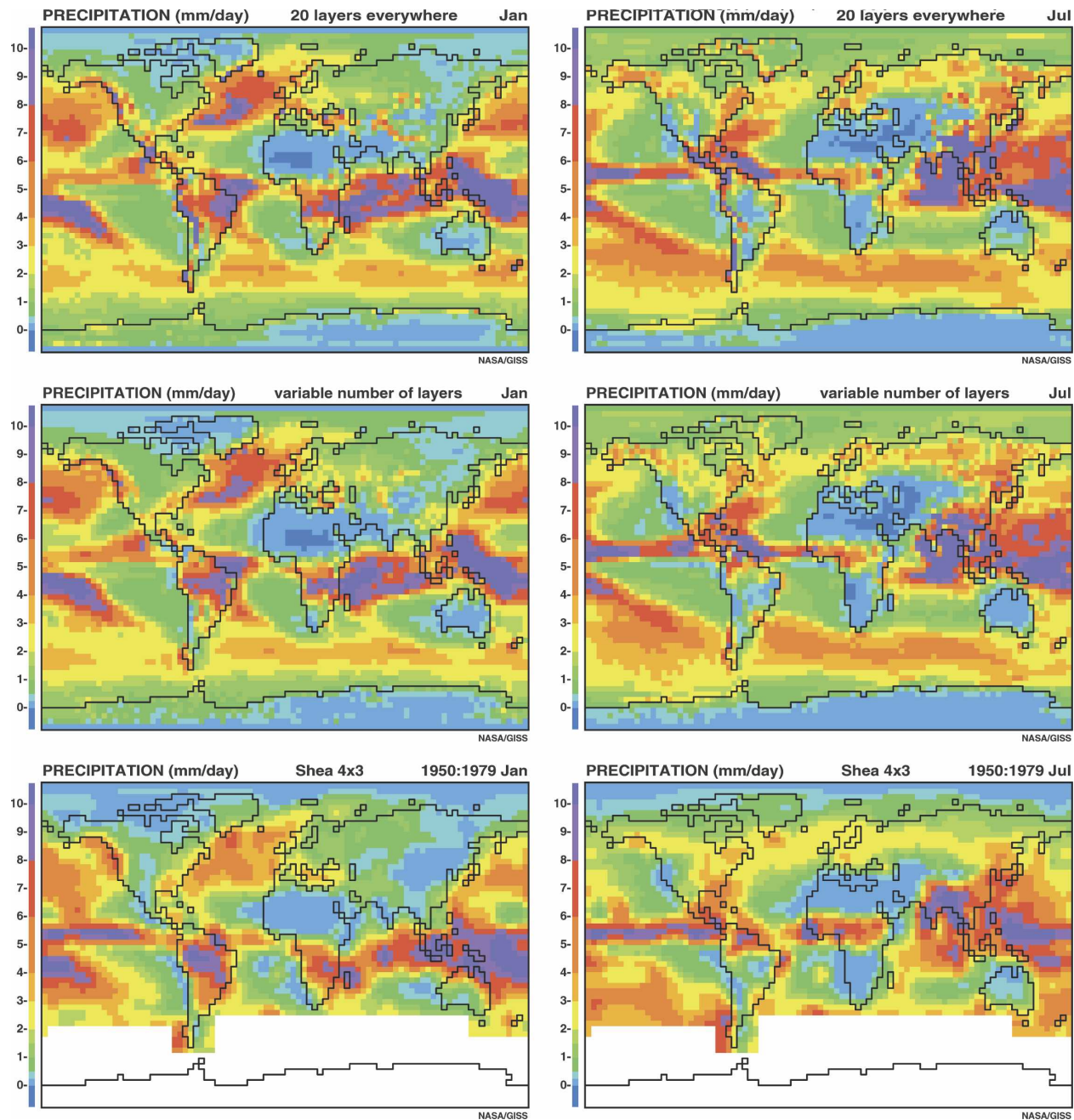


FIG. 4. Precipitation from simulations (i) and (ii) and from Shea (1986).

that if one wishes to compare with other models, coarser resolution reduces the root-mean-square errors among the observational files. The errors for  $5^{\circ} \times 4^{\circ}$  resolution are on average 3% less in January and 15% less in July than those given in Table 2.

## 11. Discussion

The purpose of discarding grid cells at the bottom of mountainous columns and modifying the topography is

to cause the mass per unit area of horizontally adjacent cells to be more nearly equal, which, according to section 2, should reduce the systematic numerical errors of horizontal momentum advection. Implementing step-mountain technique consequently improves the vertical mass fluxes and the flow around mountains. There are two reasons that the precipitation distribution is improved, especially so in the Andes. First, the vertical mass flux, which is less in error, is an important deter-

minate in large-scale condensation. Second, in a sigma coordinate model or model (i), moist air above the Pacific Ocean can jump to the top of the Andes in one step because the lowest cells are in the same layer; in model (ii), moist air must rise over the ocean, where it may condense, before moving over to the Andes.

The resultant C-grid model here is ideal for implementing step-mountain technology in terms of the mass stencil. In B-grid and E-grid schemes, velocity components are centered at the corner of four primary grid cells, and the mass of those four cells are used to convert velocity to momentum. If one or two of them become discarded mountainous cells, then the velocity must either be set to zero (which may not be desirable) or some other inelegant arrangement must be made for the mass stencil. With Arakawa and Lamb's (1977) six-cell mass stencil for the C-grid, the problem is even worse. The simplified advection scheme expounded here, with its simple two-cell mass stencil, is ideal; if one of the mass cells was discarded, then the velocity component is set to zero, being perpendicular to the face of the mountain.

Intelligent upstream schemes for nonlinear advection may some day surpass center-differencing schemes whose improvements are nearing their end. Fourth-order differencing schemes did not make improvements at GISS. They work well for simulating smooth patterns like Rossby–Haurwitz waves or stratospheric flow, but are worse than second-order schemes when local oddities occur, like sharp mountains or point source heating. A fourth-order version (Takano and Wurtele 1982) of Arakawa's potential enstrophy conserving scheme was the best among several shallow water equation models tested with Rossby–Haurwitz waves (Russell et al. 1987), but it never worked well in earth climate models. Using potential temperature as the vertical coordinate was also suggested. It would cause large variations in the mass per unit area of layers and is unlikely to make an improvement, but it was never tested.

Many things are improved by increasing resolution, but simulated flow around mountains may degrade because the horizontal topography gradients increase. While other model diagnostics became more realistic, precipitation degraded as horizontal resolution increased at GISS. Much effort and money was spent on the condensation subroutines, but errors in the basic patterns of flow prevented improvement. This problem has now been solved by using the step-mountain technique. Over the next few years, this correction of the basic pattern of flow will spread to improvements in condensation, clouds, radiation, and other aspects of the model.

When Mesinger set out to develop the eta coordinate

and the step-mountain technique, his purpose was to reduce errors in the pressure gradient force. In its simple form, the left-hand side of (C1) has two terms that are added together, the gradient of pressure and the gradient of height. Consider a column in the Pacific Ocean and an adjacent column in the Andes in a sigma coordinate system or in the hybrid model (i) with the same number of layers everywhere. The gradient of pressure accelerates the eastward velocity while the gradient of height decelerates it. The simple view of the problem (Smagorinsky et al. 1967) is that each of these terms is huge, but they nearly cancel causing the relative error to increase. Mesinger et al. (1988) are more subtle in their understanding of the problem, namely that temperatures in the Pacific column that are below the applied velocity cell's pressure are ignored in calculating the geopotential heights while temperatures in the Andes column that are above that pressure are used, both being wrong from the physical point of view. With the step-mountain technique implemented, the pressures and heights of horizontally adjacent cells are more similar, the gradients are weaker, the net calculation is no longer orders of magnitude smaller than either of the terms, and the temperature error mentioned above is nearly eliminated. The present paper agrees with the improvements to the pressure gradient force, but it claims that there is another reason to implement step-mountain, namely that systematic errors in the advection of momentum are reduced when the mass per unit areas of adjacent cells are more nearly equal. When Wyman (1996), in his E-grid step-mountain model, modified his continental topography to one of eleven possible values in order to reduce the gradient of height, he did not minimize the mass per unit area of adjacent cells as effectively as was done in section 9 here. This may be a minor point, and based on the next paragraph, the choice of method to modify the continental topography may be mute.

There is still one aspect of this paper that is unsettling: why is simulation (ii) superior to simulation (iii)? The tuning of each model is extremely similar and it seems unlikely that tuning is the cause of the discrepancy. The reason may be that small topography gradients that affect the general circulation are present in (ii), but have been removed in (iii) by the topography adjustment. The improvement in vertical mass fluxes in (iii) over those in (ii) does confirm the theoretical analysis of Russell and Lerner (1981) that mass variations are a cause of numerical errors in advection by center-difference schemes. But wiping out topography gradients to achieve this end may be counterproductive. At GISS, we now use simulations like (ii) and do not adjust the continental topography.

Gallus and Klemp (2000) using a two-dimensional model (one vertical and one horizontal direction) have pointed out deficiencies in the step-mountain technique, namely that “flow will not properly descend along the lee slope. Rather, the flow separates downstream of the mountain and creates a zone of artificially weak flow along the lee slope.” Their criticism applies to step-mountain three-dimensional schemes of the B-grid, C-grid, and E-grid, which look identical in two dimensions. When a ridge exists, the criticism is valid for all three grids, but when there is flow around a mountain, the various three-dimensional schemes will behave differently. F. Mesinger and D. Jovic (2004, unpublished manuscript) have developed a version of the eta coordinate E-grid scheme that allows sloping horizontal transport between different layers at the bottom of the atmosphere. This may eliminate the ridge problem, but it is not implemented here.

Step-mountain technology may be a benefit to E-grid and B-grid schemes, but it is a true savior to the C-grid. The improvements are truly significant. The question remains, do they restore Arakawa’s original belief that the C-grid is the best of the gridpoint schemes?

*Acknowledgments.* The author thanks Fedor Mesinger for numerous suggestions for the manuscript and for inventing the step-mountain technique in the first place. Maxwell Kelley first suggested using a single horizontal velocity vector at the poles and checking the distances used by the pressure gradient force.

## APPENDIX A

### Primitive Equations

After discretizing the vertical coordinate, the form of the primitive equations without the source terms for each layer  $L$  (counted downward) on the spherical grid are.

$$\begin{aligned} \delta M/\delta t + (\delta MU/\delta \lambda + \delta MV \cos \varphi/\delta \varphi)/R \cos \varphi \\ + W_{L+1/2} - W_{L-1/2} = 0 \end{aligned} \quad (\text{A.1})$$

$$\begin{aligned} \delta UM/\delta t + (\delta UMU/\delta \lambda + \delta UMV \cos \varphi/\delta \varphi)/R \cos \varphi \\ + (UW)_{L+1/2} - (UW)_{L-1/2} \\ - (f + U \tan \varphi/R)MV + M[\delta(\Phi + CT)/\delta \lambda \\ - (P/P_0)^\kappa \delta H/\delta \lambda]/R \cos \varphi = 0 \end{aligned} \quad (\text{A.2})$$

$$\begin{aligned} \delta VM/\delta t + (\delta VMU/\delta \lambda + \delta VMV \cos \varphi/\delta \varphi)/R \cos \varphi \\ + (VW)_{L+1/2} - (VW)_{L-1/2} \\ + (f + U \tan \varphi/R)MU + M[\delta(\Phi + CT)/\delta \varphi \\ - (P/P_0)^\kappa \delta H/\delta \varphi]/R = 0 \end{aligned} \quad (\text{A.3})$$

$$\begin{aligned} \delta QM/\delta t + (\delta QMU/\delta \lambda + \delta QMV \cos \varphi/\delta \varphi)/R \cos \varphi \\ + (QW)_{L+1/2} - (QW)_{L-1/2} = 0 \end{aligned} \quad (\text{A.4})$$

where  $M$  ( $\text{kg m}^{-2}$ ) is mass per unit area,  $U$  ( $\text{m s}^{-1}$ ) is the eastward (zonal) velocity component,  $V$  ( $\text{m s}^{-1}$ ) is the northward (meridional) velocity component,  $t$  (s) is time,  $\lambda$  is longitude,  $\varphi$  is latitude,  $R$  (m) is the radius of the earth,  $W$  ( $\text{kg m}^{-2} \text{ s}^{-1}$ ) is the downward vertical mass flux defined at layer edges,  $f$  ( $\text{s}^{-1}$ ) is the Coriolis parameter  $2\Omega \sin \varphi$  ( $\Omega$  is angular rotation rate of earth),  $\Phi$  ( $\text{m}^2 \text{ s}^{-2}$ ) is the geopotential,  $C$  ( $\text{J kg}^{-1} \text{ K}^{-1}$ ) is the specific heat capacity of dry air at constant pressure,  $T$  (K) is temperature,  $P$  (Pa) is pressure,  $P_0$  (Pa) is the fixed arbitrary reference pressure for potential quantities (e.g., temperature),  $\kappa$  is the exponent of the Exner function used in obtaining potential temperature,  $H$  ( $\text{J kg}^{-1}$ ) is potential specific enthalpy, and  $Q$  is the tracer concentration such as specific humidity or potential specific enthalpy.

## APPENDIX B

### Finite-Difference Algorithm for Simplified Advection Scheme

Finite-difference algorithms for the simplified advection scheme, the polar velocity, and the Coriolis and metric terms are described below. The momentum advection scheme and polar velocity are simpler than that described in Arakawa and Lamb (1977). Derivation of the complicated Coriolis and metric terms can be found online (see <http://aom.giss.nasa.gov/DOC4X3/CORIOLIS.TXT>).

#### a. Constants

- IM = number of longitudinal grid cells
- JM = number of latitudinal grid cells
- $R$  = radius (m) of earth
- $\Omega$  = angular rotation rate (1/s) of earth
- $d\lambda$  = longitudinal spacing of grid cells =  $2\pi/\text{IM}$
- $d\varphi$  = latitudinal spacing of grid cells =  $\pi/\text{JM}$
- $dt$  = advective time step(s)

#### b. Trigonometric functions of longitude

- $\text{COSI}_I = \cos[d\lambda (I - 1/2)]$
- $\text{SINI}_I = \sin[d\lambda (I - 1/2)]$
- $\text{COSU}_{J+1/2} = \cos(d\lambda I)$
- $\text{SINU}_{J+1/2} = \sin(d\lambda I)$

#### c. Trigonometric and distance functions of latitude

- $\text{COSV}_{J+1/2} = \cos\{d\varphi [J + 1/2 - (1 + \text{JM})/2]\}$
- $\text{SINV}_{J+1/2} = \sin\{d\varphi [J + 1/2 - (1 + \text{JM})/2]\}$
- $\text{DXYP}_J = \text{area of primary cell (m}^2\text{)}$
- $= d\lambda R^2 (\text{SINV}_{J+1/2} - \text{SINV}_{J-1/2})$

$$\begin{aligned} \text{DXV}_{J+1/2} &= X \text{ length (m) of primary gridcell} \\ &\text{edge} = d\lambda R \text{COSV}_{J+1/2} \\ \text{DXP}_J &= \text{average } X \text{ length (m) of primary grid} \\ &\text{cell} = (\text{DXV}_{J-1/2} + \text{DXV}_{J+1/2})/2 \\ \text{DYP}_J &= \text{average } Y \text{ length (m) of primary} \\ &\text{grid cell} = d\varphi R \\ \text{COSM}_J &= \text{selected cosine for angular} \\ &\text{momentum} = (\text{COSV}_{J-1/2} \\ &+ \text{COSV}_{J+1/2})/2 \\ \text{COSQ}_J^2 &= \text{selected cosine squared for} \\ &\text{angular momentum} \\ &= (\text{COSV}_{J-1/2}^2 + \text{COSV}_{J+1/2}^2)/2 \\ \text{SINxY}_J &= (\text{sine of latitude}) d\varphi \\ &= \text{COSV}_{J-1/2} - \text{COSV}_{J+1/2} \\ \text{TANxY}_J &= (\text{tangent of latitude}) d\varphi \\ &= \text{SINxY}_J/\text{COSM}_J \\ 0 &= \text{COSV}_{1/2} = \text{DXV}_{1/2} = \text{MV}_{I,1/2} \\ &= \text{UMVc}_{I+1/2,1/2} = \text{UMVw}_{I,1/2} \\ &= \text{UMVe}_{I,1/2} \\ 0 &= \text{COSV}_{\text{JM}+1/2} = \text{DXV}_{\text{JM}+1/2} \\ &= \text{MV}_{I,\text{JM}+1/2} = \text{UMVc}_{I+1/2,\text{JM}+1/2} \\ &= \text{UMVw}_{I,\text{JM}+1/2} = \text{UMVe}_{I,\text{JM}+1/2} \end{aligned}$$

International date line is located at  $(1/2, J)$   
 $= (\text{IM} + 1/2, J)$

South Pole is located at  $(I, 1/2)$

North Pole is located at  $(I, \text{JM} + 1/2)$

#### d. Definitions of variables

$$\begin{aligned} I, J &= \text{longitudinal and latitudinal index of} \\ &\text{primary grid cell} \\ M &= \text{mass per unit area (kg m}^{-2}\text{) of primary grid} \\ &\text{cell (identical at all longitudes at a pole)} \\ B &= \text{mass stencil (kg) for } U \text{ (identical at all} \\ &\text{longitudes at a pole)} \\ N &= \text{mass stencil (kg) for } V \\ U &= \text{eastward velocity component (m s}^{-1}\text{)} \\ V &= \text{northward velocity component (m s}^{-1}\text{)} \\ \text{USP} &= \text{velocity component (m s}^{-1}\text{) at South Pole} \\ &\text{pointing up } 90^\circ\text{W} \\ \text{VSP} &= \text{velocity component (m s}^{-1}\text{) at South Pole} \\ &\text{pointing up } 180^\circ \\ \text{UNP} &= \text{velocity component (m s}^{-1}\text{) at North Pole} \\ &\text{pointing down } 90^\circ\text{W} \\ \text{VNP} &= \text{velocity component (m s}^{-1}\text{) at North Pole} \\ &\text{pointing down } 0^\circ \\ \text{MU} &= \text{eastward mass flux (kg s}^{-1}\text{) located on } U \\ \text{MV} &= \text{northward mass flux (kg s}^{-1}\text{) located on } V \\ \text{UMU} &= \text{eastward momentum flux of } U \text{ (kg m s}^{-2}\text{)} \\ \text{UMV?} &= \text{northward momentum flux of } U \text{ (kg m s}^{-2}\text{)} \\ &(\text{?} = \text{c, w, or e}) \\ \text{VMU?} &= \text{eastward momentum flux of } V \text{ (kg m s}^{-2}\text{)} \\ &(\text{?} = \text{c, s, or n}) \\ \text{VMV} &= \text{northward momentum flux of } V \text{ (kg m s}^{-2}\text{)} \end{aligned}$$

#### e. $U$ at poles

$$\begin{aligned} U_{I+1/2,1} &= \text{COSU}_{I+1/2}\text{USP} - \text{SINU}_{I+1/2}\text{VSP} \\ U_{I+1/2,\text{JM}} &= \text{COSU}_{I+1/2}\text{UNP} + \text{SINU}_{I+1/2}\text{VNP} \end{aligned}$$

#### f. $V$ at poles

$$\begin{aligned} V_{I,1/2} &= \text{COSI}_I\text{VSP} + \text{SINI}_I\text{USP} \\ V_{I,\text{JM}+1/2} &= \text{COSI}_I\text{VNP} - \text{SINI}_I\text{UNP} \end{aligned}$$

#### g. Mass stencil of $U$

$$B_{I+1/2,J} = (M_{I,J} + M_{I+1,J})\text{DXYP}_J/2$$

#### h. Mass stencil of $V$

$$N_{I,J+1/2} = (M_{I,J}\text{DXYP}_J + M_{I,J+1}\text{DXYP}_{J+1})/2$$

#### i. Eastward mass flux

$$\text{MU}_{I+1/2,J} = (M_{I,J} + M_{I+1,J})\text{filtered}(U_{I+1/2,J})\text{DYP}_J/2$$

Polar filter is applied to  $U$  when calculating  $\text{MU}$ . At Poles, compute  $\text{MU}$  so that horizontal mass convergence into each polar triangle is the same for all longitudes, and summation over longitude of  $\text{MU}$  is 0. Here  $\text{MU}_{I+1/2,1}$  is a function of all  $\text{MV}_{I,3/2}$  in row, and  $\text{MU}_{I+1/2,\text{JM}}$  is a function of all  $\text{MV}_{I,\text{JM}-1/2}$  in row.

#### j. Northward mass flux

$$\text{MV}_{I,J+1/2} = (M_{I,J} + M_{I,J+1})V_{I,J+1/2}\text{DXV}_{J+1/2}/2$$

#### k. Eastward momentum flux of $U$ from $U_{I-1/2,J}$ to $U_{I+1/2,J}$

$$\text{UMU}_{I,J} = (\text{MU}_{I-1/2,J} + \text{MU}_{I+1/2,J})(U_{I-1/2,J} + U_{I+1/2,J})/4$$

#### l. Northward momentum flux of $U$ from $U_{I+1/2,J}$ to $U_{I-1/2,J+1}$ , $U_{I+1/2,J+1}$ , or $U_{I+3/2,J+1}$

$$\begin{aligned} \text{UMVw}_{I,J+1/2} &= \text{MV}_{I,J+1/2}(U_{I+1/2,J} + U_{I-1/2,J+1})/12 \\ \text{UMVc}_{I+1/2,J+1/2} &= (\text{MV}_{I,J+1/2} + \text{MV}_{I+1,J+1/2}) \\ &(U_{I+1/2,J} + U_{I+1/2,J+1})/6 \\ \text{UMVe}_{I+1,J+1/2} &= \text{MV}_{I+1,J+1/2}(U_{I+1/2,J} + U_{I+3/2,J+1})/12 \end{aligned}$$

#### m. Eastward momentum flux of $V$ from $V_{I,J+1/2}$ to $V_{I+1,J-1/2}$ , $V_{I+1,J+1/2}$ , or $V_{I+1,J+3/2}$

$$\begin{aligned} \text{VMUs}_{I+1/2,J} &= \text{MU}_{I+1/2,J}(V_{I,J+1/2} + V_{I+1,J-1/2})/12 \\ \text{VMUc}_{I+1/2,J+1/2} &= (\text{MU}_{I+1/2,J} + \text{MU}_{I+1/2,J+1}) \\ &(V_{I,J+1/2} + V_{I+1,J+1/2})/6 \\ \text{VMUn}_{I+1/2,J+1} &= \text{MU}_{I+1/2,J+1}(V_{I,J+1/2} + V_{I+1,J+3/2})/12 \end{aligned}$$

n. Northward momentum flux of  $V$  from  $V_{I,J-1/2}$  to  $V_{I,J+1/2}$

$$\text{VMV}_{I,J} = (\text{MV}_{I,J-1/2} + \text{MV}_{I,J+1/2})(V_{I,J-1/2} + V_{I,J+1/2})/4$$

o. Updated  $M$ ; Note:  $M_{\text{new}}$  is identical at all longitudes at poles

$$\begin{aligned} M_{\text{new},I,J} \text{DXYP}_J &= M_{I,J} \text{DXYP}_J + dt(\text{MU}_{I-1/2,J} \\ &\quad - \text{MU}_{I+1/2,J} + \text{MV}_{I,J-1/2} \\ &\quad - \text{MV}_{I,J+1/2}) \end{aligned}$$

p. Updated  $B$ ; Note:  $B_{\text{new}}$  is identical at all longitudes at poles

$$B_{\text{new},I+1/2,J} = (M_{\text{new},I,J} + M_{\text{new},I+1,J}) \text{DXYP}_J / 2$$

q. Updated  $N$ ;  $J + 1/2 = 3/2$ ,  $JM - 1/2$

$$\begin{aligned} N_{\text{new},I,J+1/2} &= (M_{\text{new},I,J} \text{DXYP}_J \\ &\quad + M_{\text{new},I,J+1} \text{DXYP}_{J+1}) / 2 \end{aligned}$$

r. Updated  $U$  including advection, Coriolis, and metric terms

$$\begin{aligned} U_{\text{new},I+1/2,J} B_{\text{new},I+1/2,J} &= U_{I+1/2,J} B_{I+1/2,J} + dt\{\text{UMU}_{I,J} - \text{UMU}_{I+1,J} \\ &\quad + \text{UMVe}_{I,J-1/2} + \text{UMVc}_{I+1/2,J-1/2} + \text{UMVw}_{I+1,J-1/2} \\ &\quad - \text{UMVw}_{I,J+1/2} - \text{UMVc}_{I+1/2,J+1/2} - \text{UMVe}_{I+1,J+1/2} \\ &\quad + \Omega R \text{SIN}xY_J (\text{MV}_{I,J-1/2} + \text{MV}_{I+1,J-1/2} + \text{MV}_{I,J+1/2} \\ &\quad + \text{MV}_{I+1,J+1/2})/2 + \text{TAN}xY_J (\text{UMVe}_{I,J-1/2} \\ &\quad + \text{UMVc}_{I+1/2,J-1/2} + \text{UMVw}_{I+1,J-1/2} + \text{UMVw}_{I,J+1/2} \\ &\quad + \text{UMVc}_{I+1/2,J+1/2} + \text{UMVe}_{I+1,J+1/2})/2\} \end{aligned}$$

s. Updated  $V$  including advection, Coriolis and metric terms

$$\begin{aligned} V_{\text{new},I,J+1/2} N_{\text{new},I,J+1/2} &= V_{I,J+1/2} N_{I,J+1/2} + dt\{\text{VMV}_{I,J} - \text{VMV}_{I,J+1} \\ &\quad + \text{VMU}_n_{I-1/2,J} + \text{VMU}_c_{I-1/2,J+1/2} + \text{VMU}_s_{I-1/2,J+1} \\ &\quad - \text{VMU}_s_{I+1/2,J} - \text{VMU}_c_{I+1/2,J+1/2} - \text{VMU}_n_{I+1/2,J+1} \\ &\quad - (M_{I,J} + M_{I,J+1}) \text{DXV}_{J+1/2} \times [\Omega R \text{SIN}xY_J (U_{I-1/2,J} \\ &\quad + U_{I+1/2,J}) + \Omega R \text{SIN}xY_{J+1} (U_{I-1/2,J+1} + U_{I+1/2,J+1}) \\ &\quad + (\text{TAN}xY_J U_{I-1/2,J} + \text{TAN}xY_{J+1} U_{I-1/2,J+1}) (U_{I-1/2,J} \\ &\quad + U_{I-1/2,J+1})/4 + (\text{TAN}xY_J U_{I+1/2,J} \\ &\quad + \text{TAN}xY_{J+1} U_{I+1/2,J+1}) (U_{I+1/2,J} + U_{I+1/2,J+1})/4 \\ &\quad - (\text{TAN}xY_J + \text{TAN}xY_{J+1}) (U_{I+1/2,J} - U_{I-1/2,J}) \\ &\quad \times (U_{I+1/2,J+1} - U_{I-1/2,J+1})/12\}/4, \end{aligned}$$

t. Calculate  $UP_{\text{new}}$  and  $VP_{\text{new}}$  from  $U_{\text{new}}$

$$\begin{aligned} \text{USP}_{\text{new}} &= 2 \sum (\text{U}_{\text{new},I+1/2,1} \text{COS}U_{I+1/2}) / \text{IM} \end{aligned}$$

$$\begin{aligned} \text{VSP}_{\text{new}} &= -2 \sum (\text{U}_{\text{new},I+1/2,1} \text{SIN}U_{I+1/2}) / \text{IM} \end{aligned}$$

$$\begin{aligned} \text{UNP}_{\text{new}} &= 2 \sum (\text{U}_{\text{new},I+1/2,JM} \text{COS}U_{I+1/2}) / \text{IM} \end{aligned}$$

$$\begin{aligned} \text{VNP}_{\text{new}} &= 2 \sum (\text{U}_{\text{new},I+1/2,JM} \text{SIN}U_{I+1/2}) / \text{IM} \end{aligned}$$

with the summation taken over all longitude cells in polar grid row.

## APPENDIX C

### Discretization of the Pressure Gradient Force

a. Constants

$C$  ( $\text{J kg}^{-1} \text{K}^{-1}$ ) = specific heat capacity = 1003.5 for dry air =  $\gamma/\kappa$

$G$  ( $\text{m s}^{-2}$ ) = earth's downward gravitational acceleration

$P_0$  (Pa) = reference pressure for potential quantities = 1

$\gamma$  ( $\text{J kg}^{-1} \text{K}^{-1}$ ) = gas constant = 287 for dry air =  $\kappa C$   
 $\kappa$  = exponent of exner function =  $\gamma/C$

b. Distances used in denominator of pressure gradient force

$$\Delta \text{XPGF}_J = R \Delta \lambda \int \cos^2(\varphi) d\varphi / \int \cos(\varphi) d\varphi$$

$$\Delta \text{YPGF}_{J+1/2} = R(\Phi_{J+1} - \Phi_J)$$

$$\Phi_J = \int \varphi \cos(\varphi) d\varphi / \int \cos(\varphi) d\varphi$$

= area-weighted latitude of a primary grid cell

Integrals are performed from southern edge to northern edge of primary grid cells.

c. Discrete three-dimensional prognostic variables defined on primary grid cells

$M$  (kg) = mass

$H_0$  ( $\text{J kg}^{-1}$ ) = mean potential specific enthalpy

$HZ$  ( $\text{J kg}^{-1}$ ) = vertical gradient of potential specific enthalpy times  $M/2$

d. *Derived quantities defined on primary grid columns*

- $m$  ( $\text{kg m}^{-2}$ ) = continuous downward vertical coordinate derived from  $M$   
 $\mathcal{M}$  ( $\text{kg m}^{-2}$ ) = mean value of  $m$  in cell  
 $P$  (Pa) = continuous pressure =  $Gm$   
 $\beta$  = continuous exner function =  $(P/P_0)^\kappa$   
 $\mathcal{B}$  = mass-weighted  $\beta$  in cell  
 $H$  ( $\text{J kg}^{-1}$ ) = potential specific enthalpy that is continuous within each cell =  $H_0 + 2HZ(m - \mathcal{M})/M$   
 $E$  ( $\text{J kg}^{-1}$ ) = specific enthalpy that is continuous within each cell =  $H(P/P_0)^\kappa$   
 $\mathcal{E}$  ( $\text{J kg}^{-1}$ ) = mass-weighted value of  $E$  in cell  
 $T$  (K) = temperature that is continuous within each cell =  $E/C$   
 $\alpha$  ( $\text{m}^3 \text{kg}^{-1}$ ) = specific volume from equation of state that is continuous within each cell  
 $Z$  (m) = continuous geopotential height above mean sea level by integrating the atmospheric geostrophic assumption  
 $\mathcal{Z}$  (m) = mass-weighted value of  $Z$  in cell  
 Atmospheric equation of state:  $P = \gamma T/\alpha$   
 Atmospheric geostrophic assumption:  $\delta ZG = -\alpha \delta P$

e. *Equivalent forms of the pressure gradient force*

$$\alpha \delta P / \delta X + \delta ZG / \delta X = \delta(E + ZG) / \delta X - (P/P_0)^\kappa \delta H / \delta X \quad (\text{C.1})$$

f. *Change in U by pressure gradient force*

$$\begin{aligned} \Delta(U_{I+1/2,J}) &= -dt \text{filtered}[\mathcal{E}_{I+1,J} - \mathcal{E}_{I,J} + G(Z_{I+1,J} - Z_{I,J}) \\ &\quad - (H_{0,I+1,J} - H_{0,I,J})(\mathcal{B}_{I+1,J} + \mathcal{B}_{I,J})/2] / \Delta X \text{PGF}_J \end{aligned} \quad (\text{C.2})$$

Polar filter is applied to pressure gradient force in east-west direction.

g. *Change in V by pressure gradient force*

$$\begin{aligned} \Delta(V_{I,J+1/2}) &= -dt[\mathcal{E}_{I,J+1} - \mathcal{E}_{I,J} + G(Z_{I,J+1} - Z_{I,J}) \\ &\quad - (H_{0,I,J+1} - H_{0,I,J})(\mathcal{B}_{I,J+1} \\ &\quad + \mathcal{B}_{I,J})/2] / \Delta Y \text{PGF}_{J+1/2} \end{aligned} \quad (\text{C.3})$$

REFERENCES

- Abramopoulos, F., 1988: Generalized energy and potential enstrophy conserving finite difference schemes for the shallow water equations. *Mon. Wea. Rev.*, **116**, 650–662.  
 —, 1991: A new fourth-order enstrophy and energy conserving scheme. *Mon. Wea. Rev.*, **119**, 128–133.  
 Adler, R. F., and Coauthors, 2003: The Version-2 Global Precipitation Climatology Project (GPCP) monthly precipitation analysis (1979–present). *J. Hydrometeorol.*, **4**, 1147–1167.  
 Arakawa, A., 1966: Computational design for long term numerical integration of the equations of fluid motion: Two-dimensional incompressible flow. Part I. *J. Comput. Phys.*, **1**, 119–143.  
 —, 1972: Design of the UCLA general circulation model. Department of Meteorology Tech. Rep. 7, University of California, Los Angeles, 116 pp.  
 —, and V. R. Lamb, 1977: Computational design of the basic dynamical processes of the UCLA general circulation model. *General Circulation Models of the Atmosphere*, J. Chang, Ed., Vol. 17, *Methods in Computational Physics*, Academic Press, 173–265.  
 —, and —, 1981: A potential enstrophy and energy conserving scheme for the shallow water equations. *Mon. Wea. Rev.*, **109**, 18–36.  
 Gallus, W. A., Jr., and J. B. Klemp, 2000: Behavior of flow over step orography. *Mon. Wea. Rev.*, **128**, 1153–1164.  
 German Climate Research Programme, cited 2005: Global Precipitation Climatology Center. [Available online at <http://gpcp.dwd.de>.]  
 Legates, D. R., and C. J. Willmott, 1990: Mean seasonal and spatial variability in gauge-corrected, global precipitation. *Int. J. Climatol.*, **10**, 111–127.  
 Lin, S.-J., and R. B. Rood, 1997: An explicit flux-form semi-Lagrangian shallow-water model on the sphere. *Quart. J. Roy. Meteor. Soc.*, **123**, 2477–2498.  
 Mesinger, F., 1981: Horizontal advection schemes of a staggered grid—An enstrophy and energy-conserving model. *Mon. Wea. Rev.*, **109**, 467–478.  
 —, Z. I. Janjic, S. Nickovic, D. Gavrilo, and D. G. Deaven, 1988: The step-mountain coordinate: Model description and performance for cases of alpine lee cyclogenesis for a case of an Appalachian redevelopment. *Mon. Wea. Rev.*, **116**, 1493–1518.  
 New, M., M. Hulme, and P. Jones, 1999: Representing twentieth-century space-time climate variability. Part I: Development of a 1961–1990 mean monthly terrestrial climatology. *J. Climate*, **12**, 829–856.  
 Prather, M. J., 1986: Numerical advection by conservation of second-order moments. *J. Geophys. Res.*, **91**, 6671–6681.  
 Russell, G. L., and J. Lerner, 1981: A new finite-differencing scheme for the tracer transport equation. *J. Appl. Meteorol.*, **20**, 1483–1498.  
 —, K. Takano, and F. Abramopoulos, 1987: Comparison of horizontal difference schemes for the shallow water equations on a sphere. *Short- and Medium-Range Numerical Weather Prediction*, T. Matsuno, Ed., Meteorological Society of Japan, 327–336.  
 Shea, D. J., 1986: Climatological atlas: 1950–1979 surface air tem-

- perature, precipitation, sea-surface pressure, and sea-surface temperature (45 S-90 N). NCAR Tech. Note 269+STR, 35 pp.
- Smagorinsky, J., R. F. Strickler, W. E. Sangster, S. Manabe, J. L. Holloway Jr., and G. D. Hembree, 1967: Prediction experiments with a general circulation model. *Proc. Int. Symp. on Dynamics of Large Scale Atmospheric Processes*, Moscow, Russia, Izdatel'stro Nauka, 70-134.
- Takano, K., and M. G. Wurtele, 1982: A fourth order energy and potential enstrophy conserving difference scheme. Air Force Geophysics Laboratory Rep. AFGL-TR-82-0205 (NTIS AD-A126626), 87 pp.
- Van Leer, B., 1977: Towards the ultimate conservative difference scheme. IV. A new approach to numerical convection. *J. Comput. Phys.*, **23**, 276-299.
- Wyman, B. L., 1996: A step-mountain coordinate general circulation model: Description and validation of medium-range forecasts. *Mon. Wea. Rev.*, **124**, 102-121.